Data maps for material identification in helical milling by spindle power monitoring

Sughosh Deshpande, Abdallah Bouzid, Pierre Lagarrigue, Yann Landon, Anna Carla Araujo

Data maps for material identification in helical milling by spindle power monitoring

Sughosh Deshpande[1], Abdallah Bouzid[1], Pierre Lagarrigue[1], Yann Landon[1], and Anna Carla Araujo[1, *]

[1]Institut Clément Ader, Université de Toulouse, CNRS/INSA/ISAE/Mines Albi/UPS, Toulouse, France
[*]Corresponding author: Anna Carla Araujo, araujo@insa-toulouse.fr

February 21, 2023

Abstract:
Hole making on stacked aerospace materials is a major operation during aircraft assembly which poses significant challenges during manufacturing because of different material machinability. Strategies involving smart machining including adapting proper cutting conditions using real time monitoring can lead to significant improvements. This paper is a continuation of our research that uses data map methodology characterized by different specific force regions for workpiece material identification. In this article, spindle power is monitored utilizing CNC machine internal sensor during helical milling of Aluminium and Titanium alloys in a aerospace stack for estimating cutting coefficients. Our previous research addressed the material detection in circular milling of Aluminium and Titanium alloys independently using a force dynamometer. The result shows the applicability of data map technique consisting of axial force coefficients for material identification in helical milling and highlights the significance of stack sequence.

1 Introduction

Data acquisition, monitoring and feedback loop for corrective actions plays a vital role for performance optimization in smart machining strategies implemented in industries. The hardware and techniques required for data monitoring should be feasible enough for easy implementation on the shop floor without expensive investments and disturbance to current processes [1]. Data acquisition of state of the art machine tool can add significant value and are also easy to acquire without any additional accessories or hardware setup [2]. The internal sensors in the machine tool capture a variety of data and can be useful for the operator to improve productivity and tool life during machining.

Aerospace stack hole making is one such application where lot of research is being carried out in order to enhance the process productivity and hole quality [3, 4]. Each of the material layer in a stack has different machinability and properties. Using a single tool, one shot machining, for both materials is challenging. This could lead to poor hole quality and lower production rates. The methodology of adapting cutting parameters after identification of different materials in real time can increase productivity. This can be achieved by real time force and power monitoring, data acquisition and implementing a feedback loop [5]. Pardo et al [6] discusses decision making algorithms in order to identify process incidences in stack drilling. Monitoring of signals from AE sensors for tool position identification in Carbon Fibre Reinforced Plastics (CFRP)/Aluminium stacks is shown by Neugebaur et al [7]. Fang et al [8] developed force sensor less method to detect stack interface in robotic orbital drilling operations which can be helpful to adapt proper cutting conditions.

Helical milling (also called orbital drilling) is a hole making technique, especially advantageous, for machining of hard and exotic materials resulting in better hole quality and tool life compared to axial drilling [9]. The exit burs produced in helical milling is considerably less compared to axial drilling [10]. Sun et al [11] showed higher fatigue life and surface finish for holes produced in helical milling in comparison with axial drilling of Aluminium and Titanium alloys. Better chip evacuation, less cutting forces result in better tool life and hole quality in helical milling. Implementation of helical milling for producing holes in aerospace stacks is also widely researched topic and considerable work is being done in this area [12, 13].

The state of the art shows monitoring the gradient of thrust forces or cutting torque to identify the material and tool position in a stack and can be challenging especially at the interface layers. The data maps of cutting force coefficients for individual materials can have significant advantages for real time material identification especially at the material interface to clearly distinguish the materials based on specific data points [14].

This paper presents the applicability of data maps for the identification of work piece materials during helical milling of aerospace stack made of Aluminium and Titanium alloys. Experiments are done to verify the possibility of using CNC machine internal sensor to monitor spindle power for estimating cutting coefficients. The cutting force data is also monitored by a force dynamometer in order to compare with the spindle power signal especially at material transition for gradient change. In the following sections, the cutting force model, specific force coefficients and cutting power in helical milling are presented, followed by experimental set-up, results and conclusions.

2 Helical Milling

In helical milling, the tool describes a helical trajectory as shown in Fig. 1(a). The combination of tool movement in XY plane and Z plane simultaneously results in gradual removal of material for every orbital rotation of the tool (Eq.1).

$$\vec{f_z} = \vec{f_{xy}}(\text{xy plane}) + \vec{f_a}(\text{axial}) \tag{1}$$

$$P = \frac{f_a\ 2\pi R_{tt}}{f_{xy}} = \frac{f_a\ \pi(D - D_t)}{f_{xy}} \tag{2}$$

$$\alpha = \arctan \frac{P}{\pi(D-D_t)} = \arctan \frac{f_a}{f_{xy}} \tag{3}$$

$$N_{orb} = \frac{f_a\ Z\ N}{P} \tag{4}$$

The depth of material removed per orbital rotation is designated as pitch P (mm/rev) and it is a function of the feed and the radius of the trajectory R_{tt}, calculated based on the tool diameter D_t and the machined diameter D (Eq.2). The resulting ramp angle is indicated as α (Eq. 3), a function of the axial feed and the circular feed [15].

Figure 1(b) shows tool trajectory with reference to fixed Cartesian coordinate (X_m, Y_m) and rotating tool coordinate (X_t,Y_t) systems. The tool rotates around its own axis at N(rpm) spindle speed (or $\dot{\theta}_2$ rad/s) and around hole center O at N_{orb} rpm (or $\dot{\theta}_1$ rad/s) to machine the hole. The offset distance between tool center C and hole center O is designated as R_{tt} [16].

2.1 Chip geometry

Figure 2(a) shows chip generation during helical milling. There are two zones of chip generation: at the peripheral edge, that it is represented by the index 'p' in this article, and the bottom edge of the tool, represented by 'b' index. The chip thickness (h_p) at the peripheral side of the tool is similar to conventional milling process which is a function of tool revolution angle (θ_2) and feed per tooth f_z. The chip width b_p is a function of θ_2 and the axial position of the tool in the orbital rotation

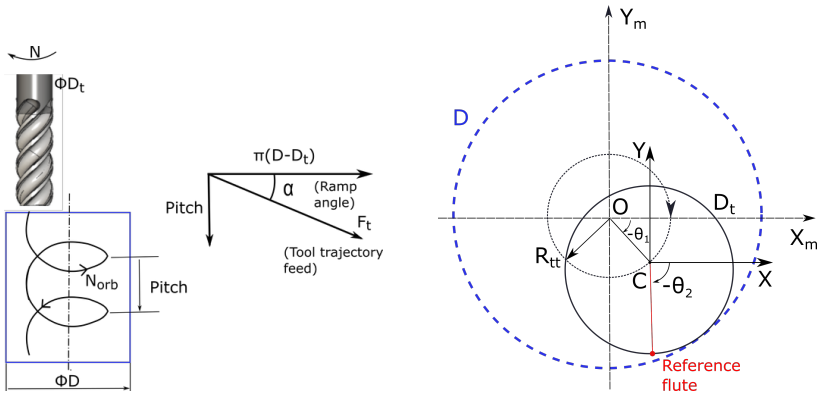

(a) Helical milling trajectory (b) Referential frames

Figure 1: Tool trajectory in helical milling.

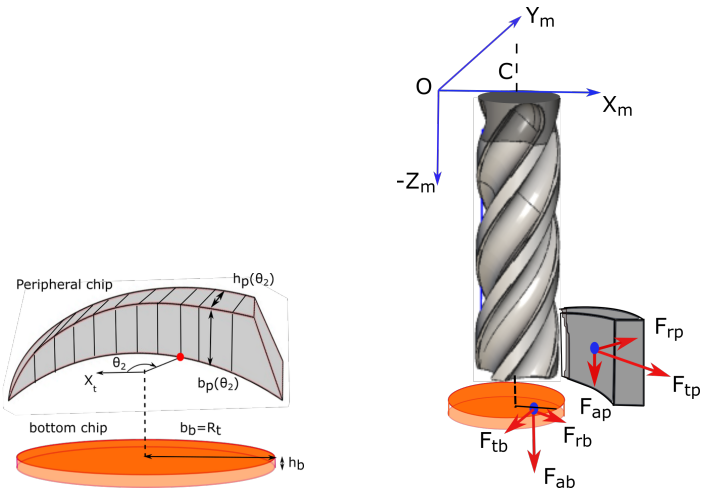

(a) Chip Geometry (b) Cutting forces

Figure 2: Chip generation and cutting forces during helical milling.

[17] and the chip thickness h_p is described by Martellotti equation [18].

$$b_p(\theta_2) = P - \frac{P}{\pi} \arccos \frac{R_{tt} - R_t \cos(\theta_2)}{\sqrt{R_{tt}^2 + R_t^2 - 2R_t R_{tt} \cos(\theta_2)}} \tag{5}$$

$$h_p(\theta_2) = f_z \sin(\theta_2) \tag{6}$$

$$b_b = \frac{D_t}{2} \tag{7}$$

$$h_b = f_z \frac{P}{\pi(D - D_t)} \tag{8}$$

In the bottom edge, the chip length b_b can be approximated to tool radius (Eq. 7) and the chip thickness h_b is described by Eq. 8. The bottom uncut chip thickness can be assumed constant and independent of cutting velocity. Hence, the specific force coefficients can be identified for the bottom edge and peripheral edge of the tool based on the local uncut chip load.

2.2 Cutting forces and coefficients

The mechanistic force models predict the cutting forces based on uncut chip load at the cutting edge. The cutting force predictions has become more and more closer to the experimental values by including various factors like tool geometry, operation type, tool vibrations etc in the force models [19]. The machining force $\vec{F}_m$ is calculated considering the small finite elements of the cutting flute in the cutting edge referential frame decomposed: tangential (dF_t), radial (dF_r) and axial (dF_z) components for the peripheral flute j is given by:

$$d\vec{F}_m = \begin{bmatrix} dF_t \\ dF_r \\ dF_a \end{bmatrix}. \tag{9}$$

Figure 2(b) illustrates the cutting forces exerted by the peripheral and bottom edges of the tool on the work piece during helical milling. The tangential, radial and axial force components are depicted at peripheral (F_{tp},F_{rp},F_{ap}) and bottom cutting edges (F_{tb}, F_{rb}, F_{ab}) respectively. However, the tangential (F_{tb}) and radial (F_{rb}) force components at the bottom edge is significantly small and can be neglected. The force components can be expressed as a function of uncut chip cross section and flute rotation angle θ_2 as:

$$F_{tp,j} = K_{tp}.h_p(\theta_2)_j b_p(\theta_2)_j \tag{10}$$
$$F_{rp,j} = K_{rp}.h_p(\theta_2)_j b_p(\theta_2)_j \tag{11}$$
$$F_{ap,j} = K_{ap}.h_p(\theta_2)_j b_p(\theta_2)_j \tag{12}$$
$$F_{ab,j} = K_{ab}.h_b R_t \tag{13}$$

where K_{tp},K_{rp},K_{ap} are the specific force coefficients for tangential, radial and axial force components obtained at peripheral cutting edge j and K_{ab} is the specific force coefficient from axial force component obtained at bottom cutting edge j. Hence the total force due to peripheral and bottom edges considering Z flutes in a tool can be expressed as below:

$$F_t = \sum_{j=1}^{Z} K_{tp}.h_p(\theta_2)_j b_p(\theta_2)_j \tag{14}$$
$$F_r = \sum_{j=1}^{Z} K_{rp}.h_p(\theta_2)_j b_p(\theta_2)_j \tag{15}$$
$$F_a = \sum_{j=1}^{Z} K_{ap}.h_p(\theta_2)_j b_p(\theta_2)_j + Z.K_{ab}.h_b R_t \tag{16}$$

However, during experiments, the cutting forces recorded are in fixed Cartesian coordinate system (F_{xm}, F_{ym}, F_{zm}) and can be transferred to one of the reference cutting edges. The reference flute position (θ_2) being known, the angular position of remaining flutes for a particular tool can be calculated:

$$(\theta_2)_j = (\theta_2) + (j-1)\lambda \tag{17}$$

where λ=$2\pi/Z$ is the tool pitch angle The axial components (F_{ap}+F_{ab}) can be approximated to cutting force (F_{zm}) obtained in Z direction during experiments. The rotation matrix for transformation of forces is given by Eq.18:

$$\begin{bmatrix} F_r(\theta_2)_j \\ -F_t(\theta_2)_j \\ F_a \end{bmatrix} = \begin{bmatrix} \cos(-\theta_2)_j & -\sin(-\theta_2)_j & 0 \\ \sin(-\theta_2)_j & \cos(-\theta_2)_j & 0 \\ 0 & 0 & 1 \end{bmatrix} . \begin{bmatrix} F_X \\ F_Y \\ F_Z \end{bmatrix} \tag{18}$$

2.3 Cutting Power

In case of end milling , depending upon the number of flutes, the cutting power is the summation of power consumed by the flutes ($j = 1...Z$) in active contact with the work piece at any instant.

$$Power_{cut} = \sum_{j=1}^{Z} [Power_p(j) + Power_b(j)] \tag{19}$$

where $Power_p$ and $Power_b$ denotes cutting power because of peripheral and bottom cutting edges respectively which are in active contact with the work piece during helical milling. Depending upon the cutter pitch angle, the number of peripheral flutes simultaneously in contact with the work piece can be determined considering peripheral angle of immersion between ϕ= 0 to 180^o for helical milling. The bottom edges of all the flutes are always in contact with the work piece during helical milling. Tangential cutting force F_{tp} at the peripheral cutting edge is the major component of cutting force in magnitude and can be considered for the calculation of cutting power $Power_p$ at peripheral edge. Similarly, axial cutting force F_{ab} is the major cutting force at the bottom edge and can be used to express cutting power $Power_b$ at bottom edge of the tool. The cutting power can be expressed approximately as a function of cutting force and cutting velocity V_c. The cutting velocity at a point on the bottom edge varies along the edge based on its distance from the tool center. Hence the cutting power is expressed as a function of average cutting velocity $\overline{V}_c$ for the bottom cutting edges as shown below:

$$Power_{cut} = \sum_{j=1}^{Z} \frac{1}{60} \Big\{ g(\theta_2) \cdot (F_{tp})_j \cdot V_c + (F_{ab})_j \cdot \overline{V}_c \Big\} \tag{20}$$

where $g(\theta_2)$=0 or 1 is a contact function based on position of the peripheral flute in or out of immersion angle zone. Tangential F_{tp} and axial F_{ab} cutting forces can be further expressed as a function of specific force coefficients (K_{tp},K_{ab}) and uncut chip load (h_p, b_p, h_b, b_b) as follows:

$$Power_{cut} = \sum_{j=1}^{Z} \frac{1}{60} \Big\{ g(\theta_2) \cdot [h_p(\theta_2) \cdot b_p(\theta_2)]_j \cdot K_{tp} \cdot V_c + [h_b \cdot b_b]_j \cdot K_{ab} \cdot \overline{V}_c \Big\} \tag{21}$$

Machine spindle power can be monitored during machining and the total spindle power monitored has components of cutting and non cutting power because of spindle inertia and power because of tool feed motion expressed as:

$$Power_{total} = Power_{idle} + Power_{cut} + Power_{feed} \tag{22}$$

The idle power component for a particular machine spindle can be determined to get the actual cutting power. The power because of tool feed motion is assumed to be relatively less in helical milling. During experiments, $power_{total}$ can be recorded at different pre defined cutting conditions. The modelled cutting power (Eq. 21) can be re-written to determine values of K_{tp} and K_{ab} as a function of cutting power and chip dimensions.

3 Materials and Methods

This section describes about the helical milling experiments conducted on Aluminium (2024A) and Titanium (Ti6Al4V) alloy stacks for a range of cutting conditions and setup as described in the following subsections. The aim of these experiments is to monitor spindle power for material identification during hole making of stacked aerospace materials by utilizing CNC machine internal sensors.

3.1 Experimental setup

Helical milling experiments were carried out on a CNC milling center DMU85-DMG mono block machine under wet condition. A carbide end mill from Fraisa (code: P45217391) with 4 flutes and 8 mm diameter was used for all the helical milling experiments (Fig.3(b)). The stack is made of Aluminium and Titanium alloy with 4 mm thickness of each layer bearing dimensions 35 mm X 100 mm. The layers are stacked together by bolt/nut assembly using a fixture as shown in the Fig. 3(a). The workpiece is fixed on a 9257B Kistler dynamometer, connected to a 5070 Kistler amplifier. Analogical data of force is converted to digital using a 9201 National Instruments acquisition module with 1000 Hz acquisition rate. For power acquisition, Sinucom NC trace software tool which can monitor spindle power at a rate of 4 ms is utilised. Along with spindle power, machine data like X, Y, Z position, spindle angular position is also recorded.

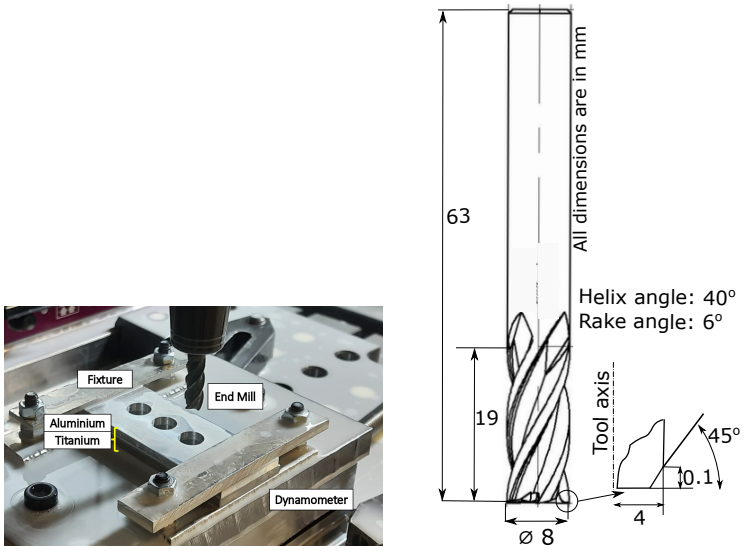

(a) Experimental setup (b) Tool details

Figure 3: Experimental details.

Table 1: Cutting conditions

Stack	f_a (mm/th)	f_z (mm/th)	V_c (m/min)	N_{orb} (rev/min)	P (mm/rev)
Ti→ Al	0.002	0.044	40	30	0.5
Ti→Al	0.003	0.059		40	
Al→Ti	0.002	0.044		30	
Al→Ti	0.003	0.059		40	
Ti→Al	0.001	0.044		30	0.3
Ti→Al	0.002	0.059		40	

3.2 Design of experiments

Table 1 summarizes the cutting conditions adopted for helical milling experiments and the corresponding stack sequence. The stack sequence is varied during experiments and represented as Al→Ti for Aluminium Titanium sequence and Ti→Al for Titanium Aluminium sequence. Cutting velocity V_c is 40 m/min (for 8mm diameter tool) in all the experiments considering machining of both material layers by the same tool and recommendations by the tool supplier. Different feed per tooth in axial (f_a) and peripheral (f_{xy}) is defined considering the resulting chip thickness and the corresponding cutting forces predicted by algorithms developed in Python. Hence, corresponding feed per tooth (f_z) at tool center point for helical trajectory is calculated along with pitch (P) and orbital rotation speed (N_{orb}) from Eq.1 to Eq. 4. The hole diameter produced is 11mm since it is one of the most popular diameters produced in aerospace industry.

4 Experimental results

The following subsections present the cutting power, cutting forces monitored during helical milling of stacks and estimated specific force coefficients data map. The specific coefficients are estimated from the cutting power signal in order to verify the possibility of utilising spindle power for material identification.

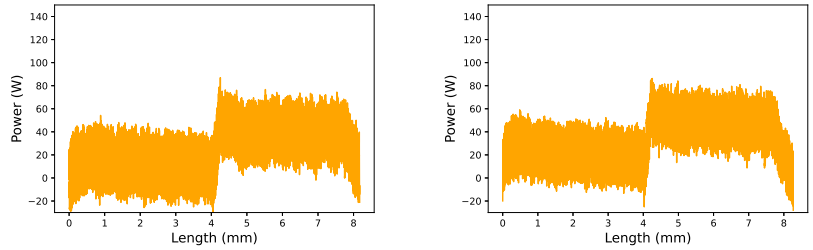

(a) Al→Ti: f_a=0.002 mm/th, f_z=0.044 mm/th

(b) Al→Ti: f_a=0.003 mm/th, f_z=0.059 mm/th

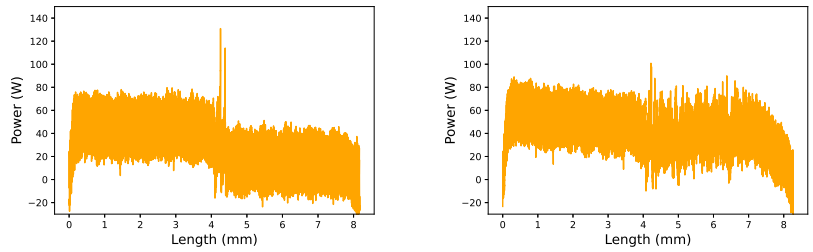

(c) Ti→Al: f_a=0.002 mm/th, f_z=0.044 mm/th

(d) Ti→Al: f_a=0.003 mm/th, f_z=0.059 mm/th

Figure 4: Cutting power with hole depth at different cutting conditions.

4.1 Cutting power

Figure 4 (a) to (d) shows cutting power as a function of hole depth at various feed per tooth and stack sequences. The material layers can be approximately identified by the distinct steps observed in the power signal at the stack interface approximately at 4 mm where tool transition occurs from one layer to other. The power signal shows disturbances while the tool is transiting from Titanium to Aluminium layer and is further observed during machining of Aluminium as shown in Fig.4 (d). This can be mostly attributed to sticky chips of Titanium sticking to the cutting edge which is re-machined while machining Aluminium. This phenomenon was also reaffirmed in the cutting force signals for Ti→Al sequences in some cases. It is important to note that these signal disturbances were not consistent for all Ti→Al stack sequence experiments but was observed frequently.

4.2 Cutting forces

Figure 5 (a) and (b) shows the cutting forces (F_t, F_r and F_a) obtained at the cutting flute after force transformation using rotation matrix for different stack sequences. However, in this article, the cutting force signals are shown only for one of the cutting conditions since the main purpose was to just compare it with the cutting power signal especially at the stack interface.

4.3 Cutting force coefficients

Cutting force coefficients K_{tp} (at tool periphery) and K_{ab} (at tool bottom edge) are estimated from cutting power signals as described in subsection 2.3. The coefficients are identified by taking maximum power values at every quarter orbital rotation of the tool and corresponding chip dimensions at that instant. K_{ab} and K_{tp} are represented as a function of hole depth for different stack sequences as shown in the Fig. 6 and 7. The data points of K_{ab} observed in Fig. 6 (a) shows distinct density of points at two regions indicating two different material layers. Density Based Spatial Clustering Algorithm (DBSCAN) is adopted in order to distinguish the data sets based on the density while removing some of the noise. Figure 6 (b) shows the data map of K_{ab} after implementing clustering model (DBSCAN) indicating data points in different symbols. Symbol (□) indicates Titanium layer

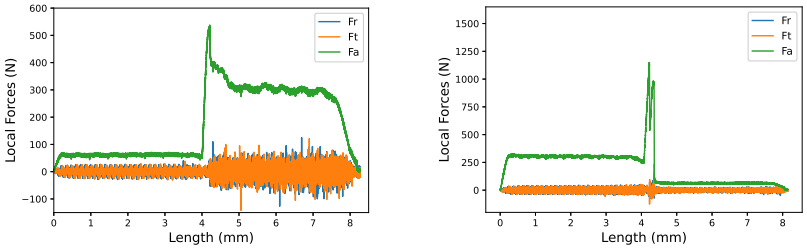

(a) Cutting forces: Al→Ti (b) Cutting forces: Ti→Al

Figure 5: Cutting force in rotating tool system as a function of hole depth at f_a=0.002 mm/th, f_z=0.044 mm/th.

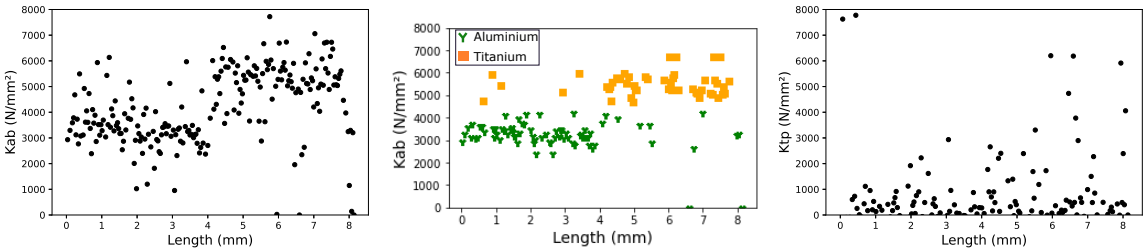

(a) K_{ab} (b) K_{ab} after DBSCAN clustering (c) K_{tp}

Figure 6: Data map of cutting force coefficients for Al→Ti stack at f_a=0.002 mm/th, f_z=0.044 mm/th

and symbol (Y) indicates Aluminium layer. The distance that specifies the neighborhoods (ϵ) value is set to 25 and minimum samples in a cluster is set to 2. The model behavior is found to be best with above parameters for our data set of K_{ab}. Figure 6 (c) shows the data map of K_{tp} as a function of hole depth and its difficult to distinguish two separate regions indicating two material layers. Figure 7 (a) shows the data map of K_{ab} for $Ti \rightarrow Al$ stack sequence and it again shows distinct region of data points. Figure 7 (b) shows data map after implementation of clustering algorithm indicating two colours for two material layers. The data map of K_{tp} is shown in Fig. 7 (c) and the indications are similar to data map of K_{tp} for $Al \rightarrow Ti$ stack sequence. It is difficult to distinguish different material layers.

5 Conclusion

The objective of this work is to check the applicability of data maps for material identification during helical milling of aerospace stacks. This is achieved by monitoring machine spindle power from the CNC machine internal sensor to estimate specific coefficients. This technique is advantageous as it does not require any external expensive sensors or any modification in the setup in order to place the sensor and is easy for shop floor implementation.

The data map of axial specific force coefficient K_{ab} makes it possible to identify the material layer in real time distinguishing two separate regions. However, it is difficult to identify two different material layers by observing data map of tangential cutting force coefficient (K_{tp}) as the data points are unevenly distributed . The stack sequence plays a crucial role in terms of generated cutting forces and required cutting power for machining. Especially, the movement of tool from Titanium to Aluminium layer is accompanied by disturbances in monitored signal of cutting force and power

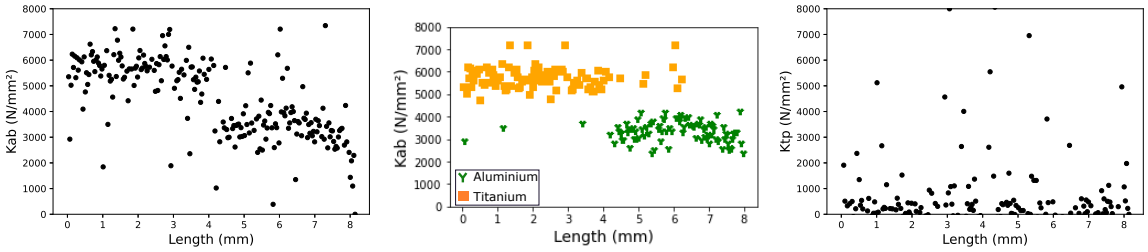

(a) K_{ab} (b) K_{ab} after DBSCAN clustering (c) K_{tp}

Figure 7: Data map of cutting force coefficients for Ti→Al stack at f_a=0.002 mm/th, f_z=0.044 mm/th

which may lead to erroneous material identification. The consequences of stack sequence on data maps needs further studies.
The map of cutting force coefficients can be grouped by clustering algorithms and can be used to train machine learning models in the future for smart machining applications including adapting optimised cutting parameter suitable for a particular layer.

References

[1] D. Axinte and N. Gindy. Assessment of the effectiveness of a spindle power signal for tool condition monitoring in machining processes. International Journal of Production Research, 42(13), jul 2004.

[2] C. H. Lauro, L. C. Brandão, D. Baldo, R. A. Reis, and J. P. Davim. Monitoring and processing signal applied in machining processes – a review. Measurement, 58:73–86, 2014.

[3] Zhu Zhaoju, Kai Liu, Jie Sun, and Jianfeng Li. Investigation on performance characteristics and metallographic transformation on drilling aluminium/titanium sandwich. Journal of Sandwich Structures and Materials, 21, August 2017.

[4] K. Vijayan, Redouane Zitoune, and Francis Collombet. Comprehensive Review on Drilling of Multimaterials Stacks. Journal of Machining and Forming Technologies, 2(3/4):171–200, 2010.

[5] Anna Carla Araujo, Yann Landon, and Pierre Lagarrigue. Smart drilling for Aerospace Industry: state of art in research and education. Procedia CIRP, 99:387–391, January 2021.

[6] Andrea Pardo, Robert Heinemann, Nuno Miguel Nobre, and Luke Bagshaw. Assessment of decision-making algorithms for adaptive drilling of aerospace stacks. Procedia CIRP, 99:392–397, January 2021.

[7] Reimund Neugebauer, Uri Ben-Hanan, Steffen Ihlenfeldt, Markus Wabner, and Andrea Stoll. Acoustic emission as a tool for identifying drill position in fiber-reinforced plastic and aluminum stacks. International Journal of Machine Tools and Manufacture, 57:20–26, June 2012.

[8] Qiang Fang, Ze-Min Pan, Bing Han, Shao-Hua Fei, Guan-Hua Xu, and Ying-Lin Ke. A Force Sensorless Method for CFRP/Ti Stack Interface Detection during Robotic Orbital Drilling Operations. Mathematical Problems in Engineering, 2015:1–11, 2015.

[9] R. Iyer, P. Koshy, and E. Ng. Helical milling: An enabling technology for hard machining precision holes in AISI D2 tool steel. International Journal of Machine Tools and Manufacture, February 2007.

[10] Jia Ge, Rincy Reji, Toby Feist, Alexander Elmore, John McClelland, Colm Higgins, Brian McLaughlin, Yan Jin, and Dan Sun. Investigating hole making performance of Al 2024-T3/Ti-6Al-4V alloy stacks: A comparative study of conventional drilling, peck drilling and helical milling. The International Journal of Advanced Manufacturing Technology, 2022.

[11] Dan Sun, Patrick Lemoine, Daniel Keys, Patrick Doyle, Savko Malinov, Qing Zhao, Xuda Qin, and Yan Jin. Hole-making processes and their impacts on the microstructure and fatigue response of aircraft alloys. The International Journal of Advanced Manufacturing Technology, February 2018.

[12] Gong-Dong Wang, Dipna Suntoo, Nan Li, Tian Peng, and Yingchi Li. Experimental research in CFRP/Ti stack through different helical milling strategies. The International Journal of Advanced Manufacturing Technology, 98:3251–3267, October 2018.

[13] B. Denkena, D. Boehnke, and J. H. Dege. Helical milling of CFRP–titanium layer compounds. CIRP Journal of Manufacturing Science and Technology, 1:64–69, January 2008.

[14] Sughosh Deshpande, Maria Clara Coimbra Gonçalves, Anna Carla Araujo, Pierre Lagarrigue, and Yann Landon. Specific force map for smart machining applications with rotating tools. Proc. Inst.of Mech. Engineers, Part B: Journal of Engineering Manufacture, 2022.

[15] Haiyan Wang, Xuda Qin, Chengzu Ren, and Qi Wang. Prediction of cutting forces in helical milling process. Int. J. of Adv. Manufacturing Technology, 58(9):849–859, February 2012.

[16] Anna Carla Araujo, Guillaume Fromentin, and Gerard Poulachon. Analytical and experimental investigations on thread milling forces in titanium alloy. Int. J. of Mac. Tools and Manufacture, 67:28–34, 2013.

[17] S. Shang, X. D. Qin, J. H. Li, S. P. Li, H. Li, T. Huang, Y. Jin, and D. Sun. Modelling of cutting forces and researching calibration method in helical milling. The International Journal of Advanced Manufacturing Technology, 94:2949–2960, February 2018.

[18] Martellotti M.E. An analysis of the milling process. Trans. ASME, pages 677–687, 1941.

[19] Y. Altintas and S. Engin. Generalized Modeling of Mechanics and Dynamics of Milling Cutters. CIRP Annals, 50:25–30, January 2001.